Approach for simultaneous measurement of two-dimensional angular distribution of charged particles. III. Fine focusing of wide-angle beams in multiple lens systems

Hiroyuki Matsuda, Hiroshi Daimon, László Tóth, and Fumihiko Matsui
Graduate School of Materials Science, Nara Institute of Science and Technology (NAIST), 8916-5 Takayama, Ikoma, Nara 630-0192, Japan and CREST, Japan Science and Technology Agency (JST), 4-1-8 Honcho, Kawaguchi, Saitama 332-0012, Japan
(Received 8 December 2006; published 20 April 2007)

This paper provides a way of focusing wide-angle charged-particle beams in multiple lens systems. In previous papers [H. Matsuda *et al.*, Phys. Rev. E **71**, 066503 (2005); **74**, 036501 (2006)], it was shown that an ellipsoidal mesh, combined with electrostatic lenses, enables correction of spherical aberration over wide acceptance angles up to ±60°. In this paper, practical situations where ordinary electron lenses are arranged behind the wide-angle electrostatic lenses are taken into account using ray tracing calculation. For practical realization of the wide-angle lens systems, the acceptance angle is set to ±50°. We note that the output beams of the wide-angle electrostatic lenses have somewhat large divergence angles which cause unacceptable or non-negligible spherical aberration in additional lenses. A solution to this problem is presented showing that lens combinations to cancel spherical aberration are available, whereby wide-angle charged-particle beams can be finely focused with considerably reduced divergence angles less than ±5°.

DOI: 10.1103/PhysRevE.75.046402 PACS number(s): 41.85.Gy, 41.85.Ne, 87.64.Lg

I. INTRODUCTION

In the previous papers [1,2], focusing of wide-angle charged-particle beams with divergence angles up to ±60° by means of an electron lens has been shown to be possible, improving the mesh lenses having been proposed [3–5]. They allow simultaneous two-dimensional (2D) angular distribution measurement of charged particles, and can provide fruitful applications in surface and materials analysis techniques such as x-ray photoelectron spectroscopy (XPS), as being of great advantage to angle-resolved XPS, photoelectron diffraction, stereo atomscopy [6], depth profiling, etc. Note that the display-type spherical mirror analyzer [7–10], while being a fine technique for simultaneous 2D angular distribution measurement [6,11–16], has a great disadvantage in that the microscopic imaging and analysis are not available because of its lensless design. The wide-angle electrostatic lenses can serve to overcome such a disadvantage, introducing the function of photoemission electron microscopy (PEEM) in the 2D angular distribution measurement.

The wide-angle electrostatic lenses proposed are of two types: an Einzel type [1] and a deceleration type [2]. In each type, an ellipsoidal mesh, together with optimized electrode arrangements, enables correction of spherical aberration over wide acceptance angles up to ±60°. A wide energy range of input beams including that in recent high-energy XPS [17,18] (in which photon energies up to around 10 keV are used) can be covered by the wide-angle electrostatic lenses without losing the capability to perform simultaneous 2D angular distribution measurement. The wide-angle deceleration lens can be suitably applied to the analysis of wide-angle high-energy charged-particle beams up to around 10 keV. The wide-angle Einzel-type lens, producing an output beam with the same kinetic energy as the initial beam, should be useful for the analysis of relatively low-energy beams.

In recent XPS, fine beam focusing is required for microscopic or nano analysis of materials [19–21]. There are some key techniques for that purpose. One technique is the aberration-canceling combination of two hemispherical analyzers [20]. A basic technique usually introduced for PEEM is the use of a cathode lens, which provides a better spatial resolution and higher electron transmission. Moreover, for aberration correction of XPS and PEEM systems, a mirror corrector [22,23] can be suitably applied, as has been used in the development of high-resolution PEEMs [24,25]. However, these techniques cannot provide fine focusing over a wide emission angle, except when the beam energy at the sample surface is extremely low compared to the cathode lens bias.

In this paper, we proceed to realize both wide angular acceptance and fine focusing in more practical situations than discussed in the previous papers [1,2]. We consider subsequent focusing of the output beams of the wide-angle electrostatic lenses, supposing that multiple lens systems are composed by arranging one or more lenses behind the wide-angle electrostatic lenses. We choose an acceptance angle of ±50° for practical realization of the wide-angle lens systems. We note that although the wide-angle electrostatic lenses can provide fine focusing at their outputs, there remain somewhat large divergence angles which cause unacceptable or non-negligible spherical aberration in additional lenses. Thus, further correction of spherical aberration is required for obtaining finely focused beams at the outputs of the multiple lens systems. We show that the wide-angle electrostatic lenses can produce the negative spherical aberrations to cancel the positive spherical aberrations of additional lenses. The consideration in this paper is responsible for developing XPS and PEEM techniques taking great advantage of the wide-angle electrostatic lenses.

II. SCHEME FOR FINE FOCUSING

A. Basic consideration

Figure 1 shows electron trajectories calculated in a typical Einzel lens. It is supposed that electrons enter the lens after

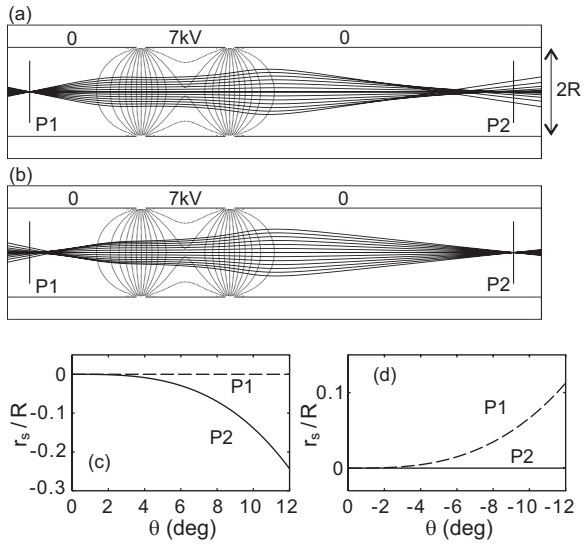

FIG. 1. Electron trajectories in a typical Einzel lens (a) starting from a point on the plane P1 and (b) converging to a point on the plane P2. The electron energy is 1 keV. The spherical aberrations r_s at P1 and P2 relative to the radius R of the lens are shown in each case, (c) and (d) corresponding to (a) and (b), respectively. Here θ is the angle of a trajectory at P1.

passing through a certain forward lens. In Fig. 1(a), no spherical aberration is produced at the image plane P1 of the forward lens. The beam divergence angle at P1 is ±12°. This results in large spherical aberration at the image plane P2 of the backward lens [see Fig. 1(c)]. In contrast, Fig. 1(b) shows electron trajectories that converge to a point on the plane P2. In this case, the negative spherical aberration canceling the positive spherical aberration of the backward lens is given at P1 [see Fig. 1(d)]. In the case of Fig. 1(a), it is possible to reduce spherical aberration by increasing the electrode voltage but, even when using a high voltage of some tens of kV for 1 keV electrons, the lens produces non-negligible spherical aberration for electrons with large incident angles of around ±10°. Therefore, we consider the scheme of Fig. 1(b) in the combination of ordinary electron lenses with the wide-angle electrostatic lenses.

B. Wide-angle Einzel-type lens

Figure 2(a) shows a four-electrode electrostatic mesh lens of the Einzel type with an acceptance angle of ±50° [1]. The mesh M, the first electrode EL1, and the final electrode EL4 are grounded. The ellipsoidal shape parameter γ (the ratio of the major radius to the minor radius of the ellipsoid) was set to $\gamma=1.73$, which minimizes spherical aberration for a certain electrode arrangement. Moreover, for fine correction of spherical aberration, the detailed adjustment of the mesh shape was done using the displacement function $\delta = \Sigma_{i=1}^{n} c_i \sin^{(p_i)} \theta \cos^{(q_i)} \theta$ (see Ref. [1]), where c_i, p_i, q_i are adjustable parameters. We set $n=4$ and adjusted the parameters until the radius of the spherical aberration disk at P1 relative to the radius R_0 of the lens entrance became less than 0.0002, which is less than 1/10 of the case of the exact ellipsoidal mesh. The difference between the obtained mesh

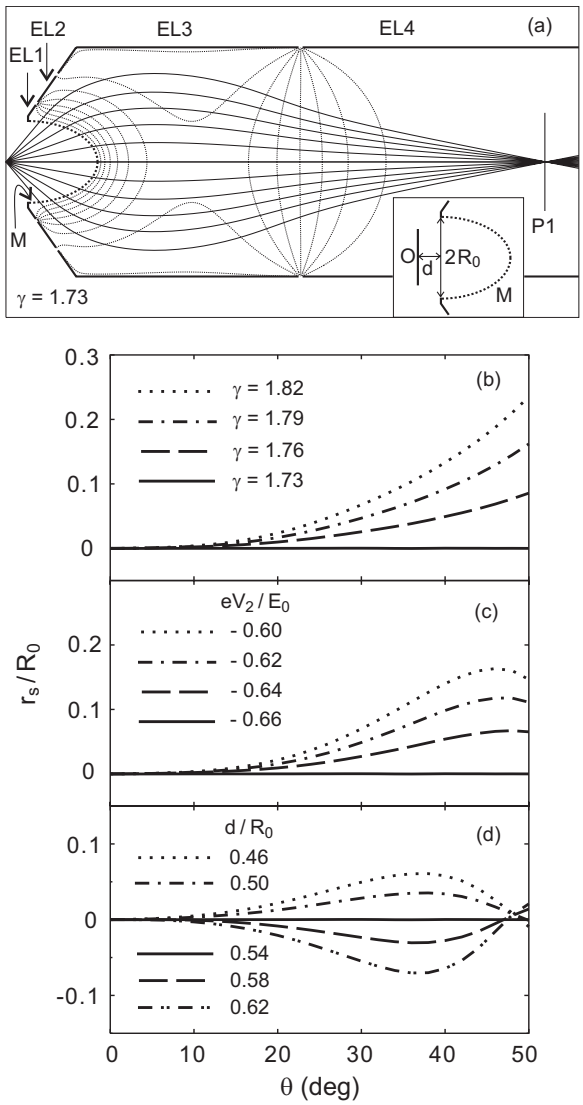

FIG. 2. Generation and control of negative spherical aberration in the wide-angle Einzel-type lens with an acceptance angle of ±50°. (a) Electron trajectories with initial angles up to ±50° in the focusing condition. Spherical aberrations r_s at P1 are shown in the variations of (b) the ellipsoidal-shape parameter γ, (c) the voltage V_2 on the second electrode EL2, and (d) the distance d between the object and the lens entrance. The solid line in each figure corresponds to the case of Fig. 2(a).

shape and the exact ellipsoidal shape is less than 0.3%. The divergence angle of the trajectories at P1 is around ±11°.

In Figs. 2(b)–2(d), the effects of the changes in the ellipsoidal shape parameter γ, the voltage V_2 on the second electrode EL2, and the distance d between the object and the lens entrance are considered. Because a change in any such parameter from the focusing condition results in a shift in the image position, we adjusted the voltage V_3 on the third electrode EL3 to give the Gaussian image plane at the same position. The solid line in Figs. 2(b)–2(d), which corresponds to the case of Fig. 2(a), shows that in the focusing condition, spherical aberration is finely corrected at the image plane P1. In Fig. 2(b), it is shown that negative spherical aberration can be well controlled by the ellipsoidal shape parameter γ.

As seen from the comparison between Fig. 1(d) and Fig. 2(b), the spherical aberration forms a nice curve at a certain increased γ for the cancellation of positive spherical aberration.

It is shown in Fig. 2(c) that it is also possible to produce negative spherical aberration by reducing the voltage V_2 on the second electrode EL2. However, the curves of the spherical aberration shown in Fig. 2(c) are not so good for the cancellation of positive spherical aberration over the full angular range. An interesting behavior of spherical aberration occurs for the variation of the distance d between the object and the lens entrance, which is shown in Fig. 2(d). It is suggested that the variation of both the voltage V_2 and the distance d may give some good negative spherical aberration at P1 for the cancellation of positive spherical aberration, even when the parameter γ is fixed at the focusing condition of the wide-angle electrostatic lens.

C. Wide-angle deceleration lens

Figure 3(a) shows a three-electrode electrostatic mesh lens of the deceleration type with an acceptance angle of ±50° [2]. The mesh M and the first electrode EL1 are grounded. The voltage V_3 on the third electrode EL3 is around −820 V for the case where the initial electron energy is 1 keV; the ratio of the final to the initial kinetic energy (the deceleration ratio) is around 0.18. The ellipsoidal shape parameter γ is given by γ=1.50. Similarly to the case of the wide-angle Einzel-type lens, the detailed adjustment of the mesh shape was performed using the displacement function δ with n=4. The obtained mesh shape is close to the exact ellipsoidal shape with γ=1.50 (the difference is less than 0.1%). The radius of the spherical aberration disk at P1 relative to the radius R_0 of the lens entrance is around 0.0002, which is around 1/5 of the case of the exact ellipsoidal mesh. The divergence angle of the trajectories at P1 is around ±11°, which is almost the same as in Fig. 2(a).

The behaviors of spherical aberration in the variations of the ellipsoidal shape parameter γ, the voltage V_2 on the second electrode EL2, and the distance d between the object and the lens entrance are shown in Figs. 3(b)–3(d). Again, negative spherical aberration can be well controlled by the ellipsoidal shape parameter γ, as shown in Fig. 3(b). Note that while the curves of spherical aberration in Fig. 3(b) are similar to those in Fig. 2(b), the changes in γ are significantly smaller than the case of the wide-angle Einzel-type lens. The spherical aberration behavior in Fig. 3(c) seems to be better than that in Fig. 2(c) for the cancellation of the positive spherical aberration of an ordinary electron lens. The spherical aberration behavior in Fig. 3(d) is similar to that in Fig. 2(d). It is seen from the comparison between Fig. 2 and Fig. 3 that the wide-angle deceleration lens is more sensitive to the parameters (γ, V_2, d) than the wide-angle Einzel-type lens, due to the fact that a focusing field of acceleration is not present in the former, while it is present in the latter.

III. LENS COMBINATION TO CANCEL SPHERICAL ABERRATION

We now proceed to the combinations of the wide-angle electrostatic lenses and ordinary electron lenses. In Fig. 4, a combination of the wide-angle Einzel-type lens and a typical three-electrode Einzel lens is considered. The electrodes EL5 and EL7 are grounded (EL4 and EL5 are at the same voltage) and a voltage of 7 kV is applied to the electrode EL6 for the case where the initial electron energy is 1 keV. Electron trajectories with initial angles up to ±50° are shown for different conditions [Figs. 4(a) and 4(b)]. In Fig. 4(a), the wide-angle Einzel-type lens is designed so that spherical aberration is finely corrected at the image plane P1, and consequently, large spherical aberration is produced at the second image plane P2. The spherical aberrations at P1 and P2 relative to the radius R_0 of the entrance of the wide-angle Einzel-type lens are shown in Fig. 4(c). The radius of the disk of least-confusion near P2 relative to R_0 is around 0.04.

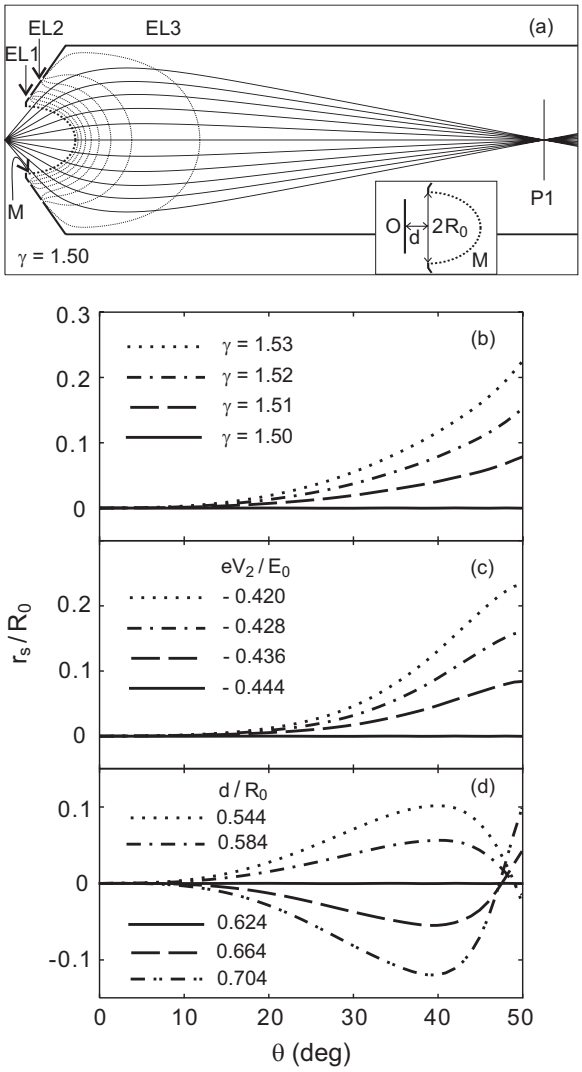

FIG. 3. Generation and control of negative spherical aberration in the wide-angle deceleration lens with an acceptance angle of ±50°. (a) Electron trajectories with initial angles up to ±50° in the focusing condition. Spherical aberrations r_s at P1 are shown in the variations of (b) the ellipsoidal shape parameter γ, (c) the voltage V_2 on the second electrode EL2, and (d) the distance d between the object and the lens entrance. The solid line in each figure corresponds to the case of Fig. 3(a).

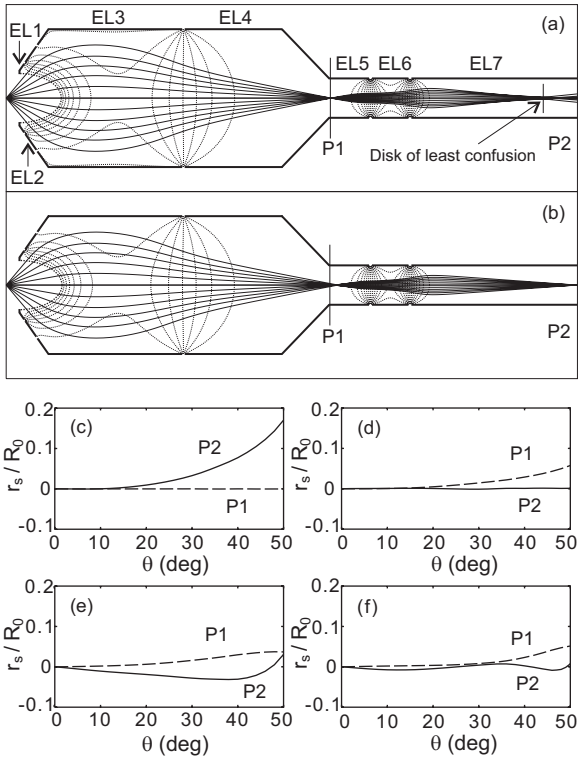

FIG. 4. Combination of the wide-angle Einzel-type lens and an ordinary Einzel lens. Electron trajectories with initial angles up to ±50° are shown in two cases: (a) Simple lens combination in which spherical aberration is corrected at P1, and (b) fine lens combination in which spherical aberration is corrected at P2. Spherical aberrations r_s at P1 and P2 are shown in different cases: (c) the case of Fig. 4(a), (d) the case of optimizing V_2 and γ, which is the case of Fig. 4(b), (e) the case of optimizing only V_2, and (f) the case of optimizing V_2 and d.

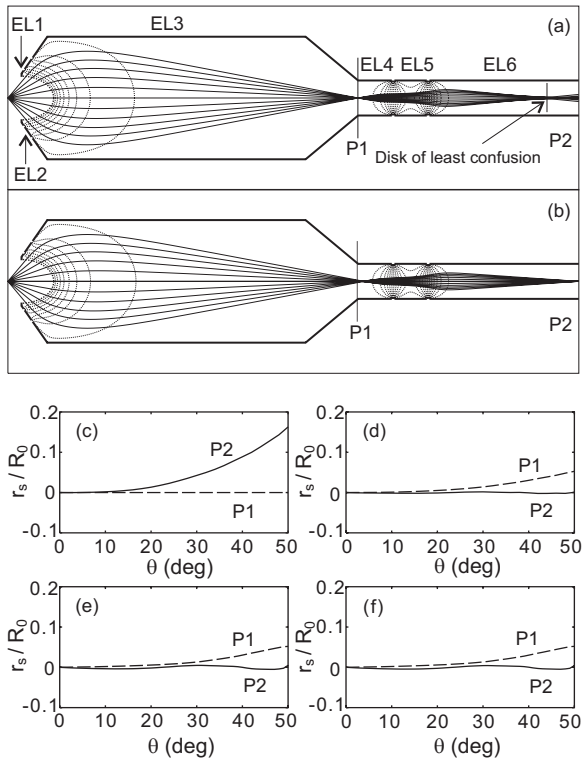

FIG. 5. Combination of the wide-angle deceleration lens and an ordinary Einzel lens. Electron trajectories with initial angles up to ±50° are shown in two cases: (a) Simple lens combination in which spherical aberration is corrected at P1, and (b) fine lens combination in which spherical aberration is corrected at P2. Spherical aberrations r_s at P1 and P2 are shown in different cases: (c) the case of Fig. 5(a), (d) the case of optimizing V_2 and γ, which is the case of Fig. 5(b), (e) the case of optimizing only V_2, and (f) the case of optimizing V_2 and d.

Figure 4(b) shows electron trajectories in an optimized lens combination. Here the ellipsoidal shape parameter γ and the voltages on the electrodes EL2 and EL3 were adjusted for fine focusing at P2; the negative spherical aberration to cancel the positive spherical aberration of the backward lens is produced at P1, as shown in Fig. 4(d). The radius of the spherical aberration disk at P2 relative to the entrance radius R_0 is around 0.001 [much smaller than that of the least-confusion disk in Fig. 4(a)]. The ellipsoidal shape parameter γ used in Fig. 4(b) is $\gamma=1.76$, while that in Fig. 4(a) is $\gamma=1.73$. The divergence angle at P2 is reasonably small, around ±4°.

The spherical aberration correction when γ is fixed at the condition of Fig. 4(a) ($\gamma=1.73$) is considered in Figs. 4(e) and 4(f). Figure 4(e) shows the result when only the voltage V_2 on EL2 is optimized from the condition of Fig. 4(a). Figure 4(f) is the result when the voltage V_2 is optimized together with the distance d between the object and the lens entrance. The spherical aberration is significantly reduced from the case of Fig. 4(e), as was suggested in the discussion of Fig. 2. However, the reduced spherical aberration is still much larger than the case of Fig. 4(d) (especially at large angles θ), which means that the adjustment of the ellipsoidal shape parameter γ is necessary for fine focusing at P2.

In Fig. 5, a combination of the wide-angle deceleration lens and a typical three-electrode Einzel lens is considered. The electrodes EL4 and EL6 are set at the same voltage as the final electrode EL3 of the wide-angle deceleration lens. A voltage of around −820 V is applied to these electrodes for the case where the initial electron energy E_0 is 1 keV. Since the electron energy reduces to βE_0 at P1 ($\beta=0.18$ in the present design), the voltage on the middle electrode EL5 of the backward lens can be much smaller than the voltage on the corresponding electrode EL6 in Fig. 4; denoting these voltages by V_A (the latter) and V_B (the former), equivalent voltages in the two cases are related by $V_B=(\beta-1)E_0/e+\beta V_A$ (e is the elementary charge). Inserting $E_0=1$ keV and $V_A=7$ kV to this equation gives $V_B=440$ V. This voltage was applied to the electrode EL5 in Fig. 5.

In Fig. 5(a), electron trajectories with initial angles up to ±50° are shown for a simple lens combination in which spherical aberration is corrected at P1 ($\gamma=1.50$); large spherical aberration is produced at P2, as shown in Fig. 5(c). Figures 5(b) and 5(d) show results for an optimized lens combination in which spherical aberration is corrected at P2; the ellipsoidal shape parameter γ and the voltage V_2 on the electrode EL2 were optimized. The γ obtained here is 1.505, slightly changed from the case of Fig. 5(a). The radius of the

spherical aberration disk at P2 relative to the entrance radius R_0 of the wide-angle deceleration lens is around 0.001. Similarly to Figs. 4(e) and 4(f), the spherical aberration correction when γ is fixed at the condition of Fig. 5(a) is considered in Figs. 5(e) and 5(f). In Fig. 5(e), the result when only the voltage V_2 is optimized is shown. The spherical aberration correction here is better than the case of the wide-angle Einzel-type lens, as expected in the previous section. No further significant reduction of spherical aberration was seen in the adjustment of the distance d between the object and the lens entrance [Fig. 5(f)].

IV. DISCUSSION AND CONCLUSION

We have presented a way of focusing wide-angle charged-particle beams in multiple lens systems. Combinations of the recently proposed wide-angle electrostatic mesh lenses [1,2] and ordinary electron lenses were considered. The wide-angle Einzel-type and deceleration lenses allow the generation and fine control of negative spherical aberration. We demonstrated that the wide-angle electrostatic lenses can indeed produce the negative spherical aberration to cancel the positive spherical aberration of an additional lens. Here, an important role can be played by the ellipsoidal shape parameter γ, the voltages on some electrodes, and the distance between the object and the lens entrance. In particular, the parameter γ is responsible for fine cancellation of positive spherical aberration; here, γ needs to be a little larger than the case where spherical aberration is independently corrected in the wide-angle electrostatic lenses. We note that the wide-angle deceleration lens allows a much lower focusing voltage on an additional lens than does the wide-angle Einzel-type lens.

In the lens combinations shown, an input beam with a divergence angle of ±50° can be transformed into a finely focused beam with a considerably reduced divergence angle of around ±4°. The output beam can be successively introduced into an XPS or PEEM lens column or a typical energy analyzer (such as a hemispherical analyzer), and can then be focused at its output. The resulting aberration can be much smaller than the case where the aberration cancellation scheme is not applied. It is thus reasonable to design wide-angle aberration-canceling lens combinations such as in this paper, adjusting all possible parameters for fine correction of spherical aberration. It is possible to simply modify the lens combinations to provide fine focusing with a further reduced divergence angle. The cancellation of the spherical aberration when two or more lenses are arranged behind the wide-angle electrostatic lenses is also possible. The proposed way of focusing wide-angle charged-particle beams in multiple lens systems is important for developing XPS and related techniques taking great advantage of the wide-angle electrostatic lenses.

[1] H. Matsuda, H. Daimon, M. Kato, and M. Kudo, Phys. Rev. E **71**, 066503 (2005).
[2] H. Matsuda and H. Daimon, Phys. Rev. E **74**, 036501 (2006).
[3] O. Scherzer, Optik (Stuttgart) **2**, 114 (1947).
[4] A. A. van Gorkum, J. Vac. Sci. Technol. B **1**, 1312 (1983).
[5] M. Kato and T. Sekine, J. Vac. Sci. Technol. A **13**, 2255 (1995).
[6] H. Daimon, Phys. Rev. Lett. **86**, 2034 (2001).
[7] H. Daimon, Rev. Sci. Instrum. **59**, 545 (1988).
[8] H. Daimon and S. Ino, Rev. Sci. Instrum. **61**, 57 (1990).
[9] H. Nishimoto, H. Daimon, S. Suga, Y. Tezuka, S. Ino, I. Kato, F. Zenitani, and H. Soezima, Rev. Sci. Instrum. **64**, 2857 (1993).
[10] T. Nohno, F. Matsui, Y. Hamada, H. Matsumoto, S. Takeda, K. Hattori, and H. Daimon, Jpn. J. Appl. Phys., Part 1 **42**, 4752 (2003).
[11] F. Matsui, Y. Hori, H. Miyata, N. Suganuma, H. Daimon, H. Totsuka, K. Ogawa, T. Furukubo, and H. Namba, Appl. Phys. Lett. **81**, 2556 (2002).
[12] F. Matsui, H. Daimon, F. Z. Guo, and T. Matsushita, Appl. Phys. Lett. **85**, 3737 (2004).
[13] F. Matsui, H. Miyata, O. Rader, Y. Hamada, Y. Nakamura, K. Nakanishi, K. Ogawa, H. Namba, and H. Daimon, Phys. Rev. B **72**, 195417 (2005).
[14] F. Z. Guo, T. Matsushita, K. Kobayashi, F. Matsui, Y. Kato, H. Daimon, M. Koyano, Y. Yamamura, T. Tsuji, and Y. Saitoh, J. Appl. Phys. **99**, 024907 (2006).
[15] Y. Kato, F. Matsui, T. Shimizu, T. Matsushita, F. Z. Guo, T. Tsuno, and H. Daimon, Sci. Technol. Adv. Mater. **7**, S45 (2006).
[16] H. Daimon and F. Matsui, Prog. Surf. Sci. **81**, 367 (2006).
[17] K. Kobayashi, M. Yabashi, Y. Takata, T. Tokushima, S. Shin, K. Tamasaku, D. Miwa, T. Ishikawa, H. Nohira, T. Hattori, Y. Sugita, O. Nakatsuka, A. Sakai, and S. Zaima, Appl. Phys. Lett. **83**, 1005 (2003).
[18] G. Beamson, S. R. Haines, N. Moslemzadeh, P. Tsakiropoulos, J. F. Watts, P. Weightman, and K. Williams, J. Electron Spectrosc. Relat. Phenom. **142**, 151 (2005).
[19] M. Merkel, M. Escher, J. Settemeyer, D. Funnemann, A. Oelsner, Ch. Ziethen, O. Schmidt, M. Klais, and G. Schönhense, Surf. Sci. **480**, 196 (2001).
[20] M. Escher, N. Weber, M. Merkel, C. Ziethen, P. Bernhard, G. Schönhense, S. Schmidt, F. Forster, F. Reinert, B. Krömker, and D. Funnemann, J. Phys.: Condens. Matter **17**, S1329 (2005).
[21] M. Escher, N. Weber, M. Merkel, B. Krömker, D. Funnemann, S. Schmidt, F. Reinert, F. Forster, S. Hüfner, P. Bernhard, Ch. Ziethen, H. J. Elmers, and G. Schönhense, J. Electron Spectrosc. Relat. Phenom. **144-147**, 1179 (2005).
[22] G. F. Rempfer, J. Appl. Phys. **67**, 6027 (1990).
[23] Z. Shao and X. D. Wu, Rev. Sci. Instrum. **61**, 1230 (1990).
[24] R. Fink *et al.*, J. Electron Spectrosc. Relat. Phenom. **84**, 231 (1997).
[25] W. Wan, J. Feng, H. A. Padmore, and D. S. Robin, Nucl. Instrum. Methods Phys. Res. A **519**, 222 (2004).